

# A Climatology of Diurnal and Semidiurnal Surface Wind Variations over the Tropical Pacific Ocean Based on the Tropical Atmosphere Ocean Moored Buoy Array

REI UEYAMA

*Department of Atmospheric Sciences, University of Washington, Seattle, Washington*

CLARA DESER

*National Center for Atmospheric Research, Boulder, Colorado*

(Manuscript received 5 September 2006, in final form 31 May 2007)

## ABSTRACT

Hourly measurements from 51 moored buoys in the Tropical Atmosphere Ocean array (9°N–8°S, 165°E–95°W) during 1993–2004 are used to document the climatological seasonal and annual mean patterns of diurnal and semidiurnal near-surface wind variability over the tropical Pacific Ocean. In all seasons, the amplitude of the semidiurnal harmonic is approximately twice as large as the diurnal harmonic for the zonal wind component, while the diurnal harmonic is at least 3 times as large as the semidiurnal harmonic for the meridional wind component, both averaged across the buoy array. Except for the eastern equatorial Pacific, the semidiurnal zonal wind harmonic exhibits uniform amplitude ( $\sim 0.14 \text{ m s}^{-1}$ ) and phase [maximum westerly wind anomalies  $\sim 0325/1525$  local time (LT)] across the basin in all seasons. This pattern is well explained by atmospheric thermal tidal theory. The semidiurnal zonal wind signal is diminished over the cold surface waters of the eastern equatorial Pacific where it is associated with enhanced boundary layer stability. Diurnal meridional wind variations tend to be out of phase north and south of the equator (maximum southerly wind anomalies  $\sim 0700$  LT at 5°N and  $\sim 1900$  LT at 5°S), while a noon southerly wind anomaly maximum is observed on the equator in the eastern Pacific particularly during the cold season (June–November). The diurnal meridional wind variations result in enhanced divergence along the equator and convergence along the southern border of the intertropical convergence zone  $\sim 0700$  LT (opposite conditions  $\sim 1900$  LT); the amplitude of the divergence diurnal cycle is  $\sim 5 \times 10^{-7} \text{ s}^{-1}$ . The diurnal meridional wind variations are largely consistent with the diurnal pressure gradient force.

## 1. Introduction

The tropical atmosphere varies on a multitude of time scales and influences weather and climate on regional and global scales. The intraseasonal Madden–Julian oscillation and the interannual El Niño–Southern Oscillation (ENSO) are two well-documented modes of variability whose effects extend beyond the tropical Pacific Ocean basin. The climate of the tropical Pacific also undergoes daily variations in, for example, barometric pressure, cloudiness, rainfall, and near-surface wind (e.g., Haurwitz and Cowley 1973; Hamilton 1980; Hendon and Woodberry 1993; Gutzler and Hartten 1995; Deser and Smith 1998; Dai and Wang 1999; Yang

and Slingo 2001; Yang and Smith 2006). These daily cycles are associated with large variations in the solar forcing and represent fundamental modes of variability in the global climate system. However, in part because of the scarcity of observational data over the oceans, much work still remains in characterizing and interpreting daily variations of tropical atmospheric properties.

Deser and Smith (1998, hereafter DS) analyzed 4 yr (1993–96) of hourly near-surface wind data from the Tropical Atmosphere Ocean (TAO) moored buoy array and showed that the mean daily march of the zonal (meridional) wind component is primarily semidiurnal (diurnal). They further noted that the phase, amplitude, and spatial pattern of the semidiurnal zonal wind variations are consistent with the classical theory of atmospheric thermal tides. Briefly, diurnal and semidiurnal atmospheric thermal tides are generated by the absorption of solar radiation by ozone in the stratosphere and water vapor in the troposphere. The tides propagate

---

*Corresponding author address:* Rei Ueyama, Department of Atmospheric Sciences, University of Washington, Box 351640, Seattle, WA 98195.

E-mail: rei@atmos.washington.edu

TABLE 1. Percent data coverage at each TAO buoy during 1993–2004 for wind, SST, and air temperature data, and during 2000–04 for pressure data. The parentheses denote less than 50% wind data coverage. A dash indicates lack of pressure measurements. For example, for the buoy at 8°N, 95°W, 43% of the wind records, 79% of the SST records, and 72% of the air temperature records during 1993–2004 have data; and 60% of the pressure records during 2000–04 have data.

	165°E	180°W	170°W	155°W	140°W	125°W	110°W	95°W
9°N	—	—	—	—	76/100/97/—	—	—	—
8°N	64/93/80/—	59/80/66/—	95/99/98/—	65/90/84/—	—	63/92/86/—	85/92/88/—	(43)/79/72/60
5°N	77/96/100/—	74/88/92/—	79/87/93/—	85/100/99/—	85/95/95/—	(40)/96/79/—	61/87/87/—	60/82/83/48
2°N	78/97/90/—	74/95/92/—	66/81/91/—	75/85/89/—	66/91/90/—	84/91/75/—	78/95/88/74	(38)/67/61/37
0°	(44)/80/67/—	79/94/92/—	90/99/95/—	93/99/92/—	91/96/92/—	76/90/89/—	65/91/79/68	64/79/78/53
2°S	63/83/90/—	93/98/98/—	72/96/84/—	71/86/83/—	81/98/98/—	92/99/89/—	68/94/91/25	56/86/83/48
5°S	53/95/90/—	66/91/87/—	78/92/92/—	90/99/91/—	100/100/100/—	95/95/95/—	76/89/88/—	68/76/76/37
8°S	66/87/88/—	83/83/88/—	88/91/95/—	86/100/97/—	—	77/94/84/—	78/97/91/—	76/79/81/55

downward to the earth's surface, affecting sea level pressure and thereby surface winds. Tidal signals observed at the surface are mainly semidiurnal (Chapman and Lindzen 1970) because the energy of the diurnal forcing is trapped near the level of excitation in the lower stratosphere and upper troposphere (Haurwitz 1964; Lindzen 1967). In particular, the semidiurnal component of the sea level pressure tidal amplitude over the tropics is 2–3 times larger than the diurnal component. While the semidiurnal zonal wind variations documented by DS are consistent with atmospheric thermal tidal theory, the observed diurnal meridional wind variations over the tropical Pacific have yet to be explained, although we note that tidal theory may also be relevant.

The diurnal cycle in tropical convection is clearly important for understanding the diurnal variability in the surface wind field. Many studies have documented the diurnal cycles in deep convection and rainfall over the tropical oceans from a variety of data sources including satellite products from the Tropical Rainfall Measuring Mission (Bowman et al. 2005; Yang and Smith 2006) and International Satellite Cloud Climatology Project (Hendon and Woodberry 1993), in situ ship reports from the Comprehensive Ocean Atmosphere Data Set (COADS; Janowiak et al. 1994), and rain gauges from island stations (Gray and Jacobson 1977) and the TAO buoys (Serra and McPhaden 2004). The various datasets are all broadly consistent in indicating an early morning [ $\sim$ 0300–0600 local time (LT)] rainfall maximum over the tropical oceans. Despite documentation of a clear diurnal signal in oceanic deep convective rainfall, neither its mechanism nor its connection to the diurnal cycle of surface wind and wind divergence are well understood (Yang and Smith 2006).

Given the importance of the surface wind field to the large-scale circulations of the atmosphere and ocean, this study seeks to expand our knowledge of daily (diurnal and semidiurnal) surface wind variability over the

tropical Pacific using 12 yr (1993–2004) of hourly wind data from the TAO moored buoy array. Extending earlier results of DS, we document the climatological annual and semiannual mean patterns of diurnal and semidiurnal surface wind variations.

## 2. Data and methods

### a. Data

There are  $\sim$ 55 moored TAO buoys in the tropical Pacific Ocean (9°N–8°S, 165°E–95°W) located approximately every 2°–3° of latitude and 15° of longitude. The spacing of the buoys was chosen to be commensurate with the narrow meridional scale of oceanic processes at the equator, such as equatorially trapped waves and upwelling motions that determine sea surface temperature (SST) anomalies during ENSO. This arrangement of narrow meridional spacing of the buoys is not optimal for the study of large-scale atmospheric circulation. Nevertheless, the TAO array is a valuable tool for monitoring daily variations of surface winds across the tropical Pacific because of its unprecedented spatial and temporal coverage. This study examines 12 yr (1 January 1993–31 December 2004) of hourly wind data from the 51 buoys that had at least 50% of data coverage (Table 1). For the selected buoys, the average number of days per year containing data is 278, ranging from a minimum of 193 at 5°S, 165°E to a maximum of 365 at 5°S, 140°W. These numbers account for the time span of data collection at each buoy as well as the frequent gaps in the record due to instrument failure.

The TAO array samples winds at 3.8 m above sea level. Wind speed measurements are made with a propeller and have a resolution of 0.2 m s<sup>-1</sup> and an accuracy of  $\pm$ 0.3 m s<sup>-1</sup>. A vane or a fluxgate compass is used to measure wind direction at 1.4° resolution with an accuracy of 5°–7.8°. Wind data were recorded for a 6-min interval at the beginning of each hour until 1996, after which they are recorded every 10 min.

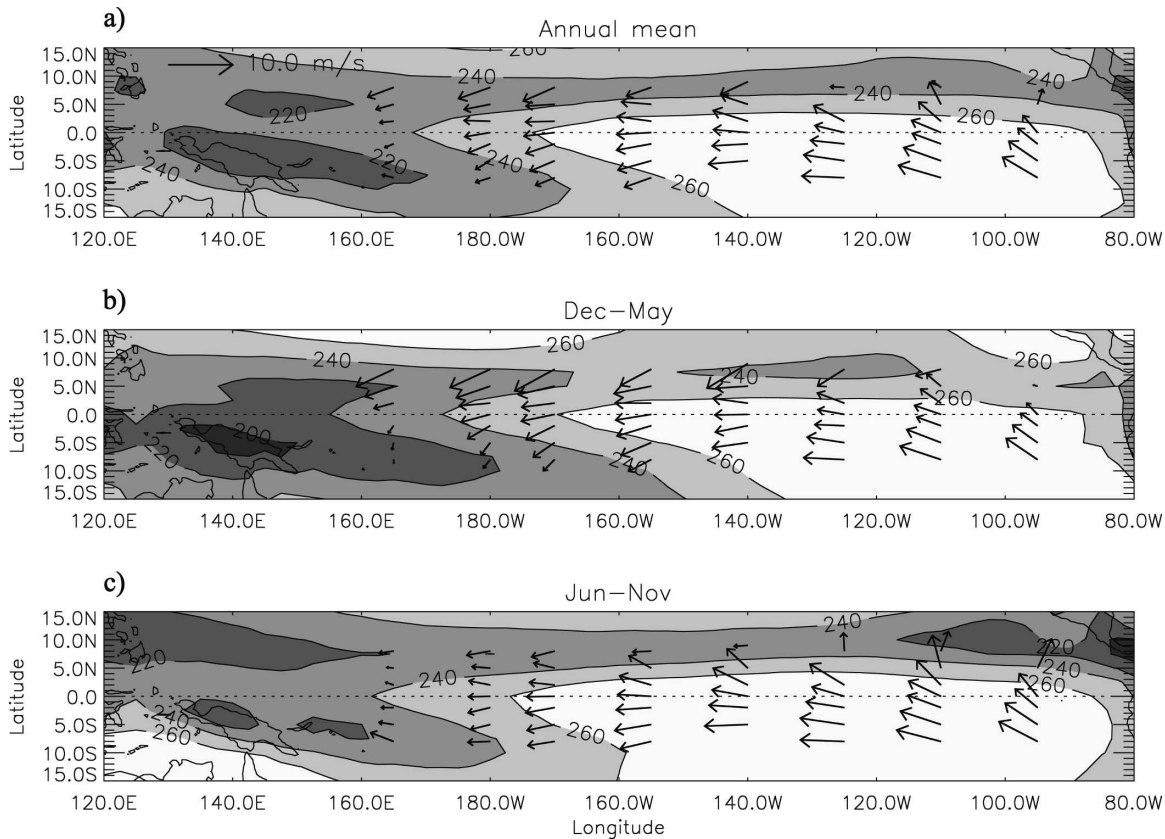


FIG. 1. Mean surface wind vectors during 1993–2004 from the TAO array superimposed on mean outgoing longwave radiation during 1997–2001 (shading and contours at  $20 \text{ W m}^{-2}$  intervals): (a) annual mean, (b) December–May, and (c) June–November. Scale at top-left corner of (a).

In addition to the wind data, hourly measurements of barometric pressure, SST, and air temperature from the TAO buoys are also examined for further analysis. Pressure data became available after 1 January 2000 when pressure sensors were added to the 10 easternmost TAO buoys along  $110^\circ$  and  $95^\circ\text{W}$  (Table 1) as part of the East Pacific Investigation of Climate (EPIC) study. Owing to this data limitation, all available pressure data between 1 January 2000 and 31 December 2004 are analyzed regardless of the low temporal coverage at some buoys (Table 1). Data coverage for SST and air temperature is high (Table 1).

Barometric pressure is measured using a pressure transducer at 3 m above sea level with 0.1-hPa resolution and an accuracy of  $\pm 0.01\%$ . SST is measured at 1 m below the sea surface using a thermistor with  $0.001^\circ\text{C}$  resolution and an accuracy of  $\pm 0.02^\circ\text{--}0.03^\circ\text{C}$ . Air temperature is measured at 3 m above sea level using a resistance temperature recorder with  $0.01^\circ\text{C}$  resolution and  $\pm 0.2^\circ\text{C}$  accuracy. Further details of the TAO array datasets can be found on the TAO Project Office Web site of the National Oceanic and Atmospheric Admin-

istration (NOAA)/Pacific Marine Environmental Laboratory (available online at <http://www.pmel.noaa.gov/tao/index.shtml>).

#### b. Methods

Seasonal (December–February, March–May, June–August, and September–November) mean daily wind marches (i.e., mean variation of wind from hour to hour over the course of a day) were computed for each buoy and year by averaging all available measurements of the two wind components at every hour within the given 3-month period. The seasonally averaged daily wind marches were then averaged over all 12 yr for each buoy. Annual and semiannual (December–May and June–November) mean marches were constructed by averaging the seasonal mean marches. Finally, the daily means of the annual and semiannual mean hourly wind marches were removed.

All annual and semiannual mean hourly wind marches constructed in this manner were decomposed into diurnal and semidiurnal harmonics following

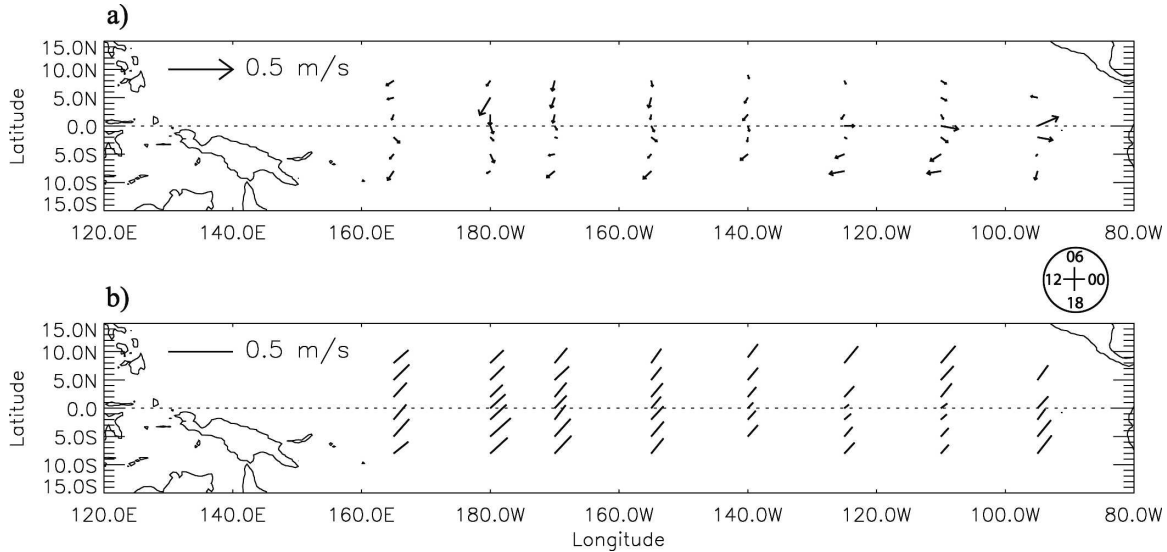


FIG. 2. Annual mean amplitudes and phases of the (a) diurnal and (b) semidiurnal harmonics of the zonal wind. The length of each vector represents amplitude of the corresponding harmonic (scale at top-left corner of both panels) and the direction represents the LT of maximum westerly wind anomaly (clock at middle right). For example, an arrow pointing due north in (a) implies maximum westerly wind anomaly at 0600 LT, and a vertical bar in (b) implies maximum westerly wind anomalies at 0600 and 1800 LT.

$$X_k(t) = A_k \cos(2\pi k/24t) + B_k \sin(2\pi k/24t), \quad (1)$$

where  $X$  denotes the zonal or meridional wind anomalies at the  $t$ th hour of the day ( $t$  in local time), with  $k$  referring to the diurnal harmonic ( $k = 1$ ) or semidiurnal harmonic ( $k = 2$ ). Here  $A$  and  $B$  are values determined by the method of least squares (Draper and Smith 1966). To portray the spatial patterns of the diurnal and semidiurnal wind variations, the amplitudes

and phases of the harmonics at each buoy are plotted on a map in vector format.

### 3. Results

#### a. Mean wind field

As background to the analysis of diurnal and semidiurnal variability, we first present the annual and semi-

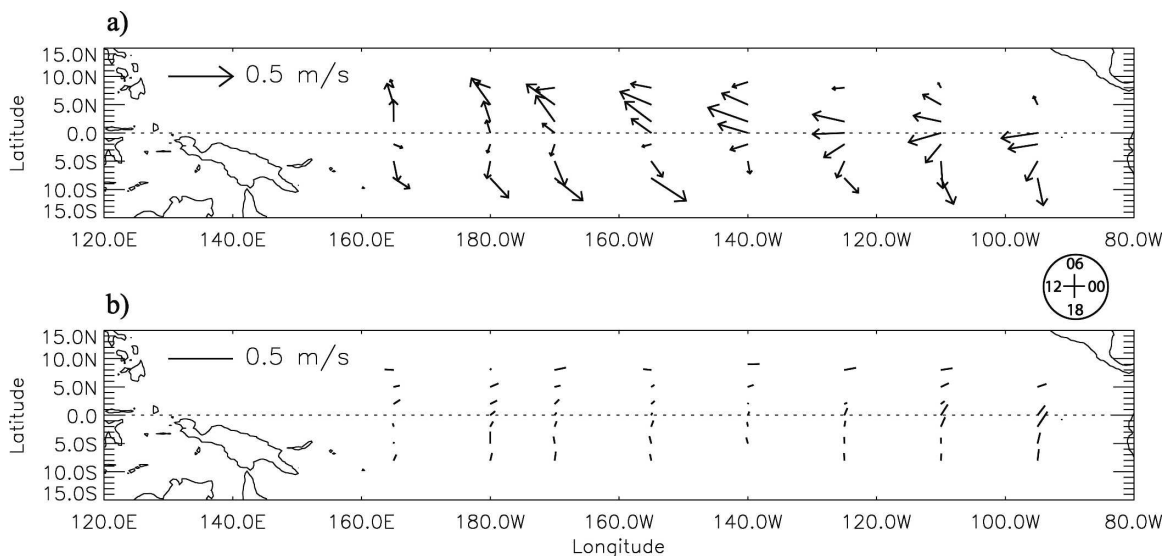


FIG. 3. Same as in Fig. 2, but for the meridional wind. The direction of the vectors represents the LT of maximum southerly wind anomaly (clock at middle right).

annual (December–May and June–November) mean wind fields from the TAO buoys during 1993–2004 (Fig. 1). December–May and June–November correspond to the warm and cold seasons, respectively, in the tropical Pacific (Wallace et al. 1989; Hartten and Datulayta 2004, hereafter HD). Surface winds are predominantly easterly across the basin throughout the year, converging into the region of deep convection (as inferred from outgoing longwave radiation values less than  $240 \text{ W m}^{-2}$ ) over the western Pacific. Surface convergence associated with the meridional component of the wind is evident within the areas of deep convection along the intertropical convergence zone (ITCZ) and the South Pacific convergence zone (SPCZ). The semiannual variation of the surface wind field is qualitatively consistent with that of deep convection, with increased meridional flow into the enhanced convective region along the ITCZ from June through November (Fig. 1c) and along the SPCZ from December through May (Fig. 1b).

#### b. Daily wind harmonics: Annual mean

Figures 2 and 3 show the annual mean amplitudes and phases of the diurnal and semidiurnal harmonics of the zonal and meridional winds, respectively. The length of the vector represents the amplitude of the harmonic at each buoy, and its direction denotes the phase in LT. Arrowheads on the bars of the diurnal harmonics of the zonal (meridional) wind point to the time of maximum westerly (southerly) wind anomaly (the term “anomaly” is used with respect to the daily mean wind). Due north indicates a maximum at 0600 LT, with time increasing in the counterclockwise direction (e.g., due west is 1200 LT, due south is 1800 LT, due east is 0000 LT). Arrowheads are not present on the bars of the semidiurnal harmonics because maximum winds occur twice a day, 12 h apart. For example, a vertical bar in the semidiurnal zonal (meridional) wind plot indicates maximum westerly (southerly) wind anomalies at 0600 and 1800 LT.

The phases and amplitudes of the semidiurnal harmonics of the zonal wind are strikingly uniform; maximum westerly wind anomalies are observed consistently  $\sim 0325/1525$  LT with amplitudes  $\sim 0.14 \text{ m s}^{-1}$  (Fig. 2b). The semidiurnal signal is weak along  $125^\circ$  and  $110^\circ\text{W}$  at and south of the equator. Diurnal variability has generally smaller amplitudes and less coherent phases than semidiurnal variability (Fig. 2a).

The daily meridional wind cycle is dominated by diurnal variability whose amplitude is approximately 3 times the amplitude of the semidiurnal variability at most buoys (Fig. 3). Diurnal variability of the meridional wind in the western Pacific ( $165^\circ\text{E}$ – $155^\circ\text{W}$ ) exhibits an approximately 12-h phase difference between

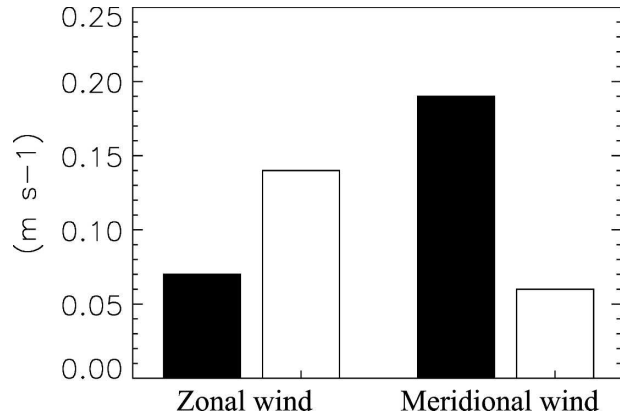


FIG. 4. Annual mean amplitudes ( $\text{m s}^{-1}$ ) of diurnal (black) and semidiurnal (white) harmonics of zonal and meridional winds averaged over the TAO buoy domain.

buoys along  $2^\circ$ – $5^\circ\text{N}$  and those along  $5^\circ$ – $8^\circ\text{S}$ ; maximum southerly wind anomalies are observed between 0600 and 0900 LT in the Northern Hemisphere, and between 1800 and 2100 LT in the Southern Hemisphere. In the eastern Pacific ( $125^\circ$ – $95^\circ\text{W}$ ), the phase propagates more gradually from north to south, with maximum southerly wind anomalies  $\sim 1000$  LT at  $5^\circ\text{N}$  progressing to  $\sim 2000$  LT at  $8^\circ\text{S}$ . Semidiurnal variations of the meridional wind, despite their small amplitudes, exhibit coherent phases with maximum southerly wind anomalies  $\sim 0000/1200$  LT ( $\sim 0600/1800$  LT) in the Northern (Southern) Hemisphere (Fig. 3b). This pattern of cross-equatorial asymmetry of the semidiurnal meridional wind anomalies is in quadrature to the semidiurnal cycle of the zonal wind (Fig. 2b) and is likely a result of the Coriolis force, as discussed in DS.

Figure 4 quantifies the relative amplitudes of the diurnal and semidiurnal harmonics of each wind component averaged across the buoy array. The mean amplitude of the semidiurnal harmonics of the zonal wind is twice as large as that of the diurnal harmonics ( $0.14$  versus  $0.07 \text{ m s}^{-1}$ ), while the mean diurnal amplitude of the meridional wind is more than 3 times as large as its mean semidiurnal amplitude ( $0.19$  versus  $0.06 \text{ m s}^{-1}$ ).

#### c. Daily wind harmonics: Semiannual means

Figures 5 and 6 show semiannual (December–May and June–November) mean amplitudes and phases of the diurnal and semidiurnal harmonics of the zonal and meridional winds, respectively. In addition to the general patterns of their annual mean counterparts, the semiannual harmonics exhibit some noteworthy differences. For example, the suppression of the semidiurnal zonal wind harmonic along  $125^\circ$  and  $110^\circ\text{W}$  at, and south of, the equator, is even more apparent in June–

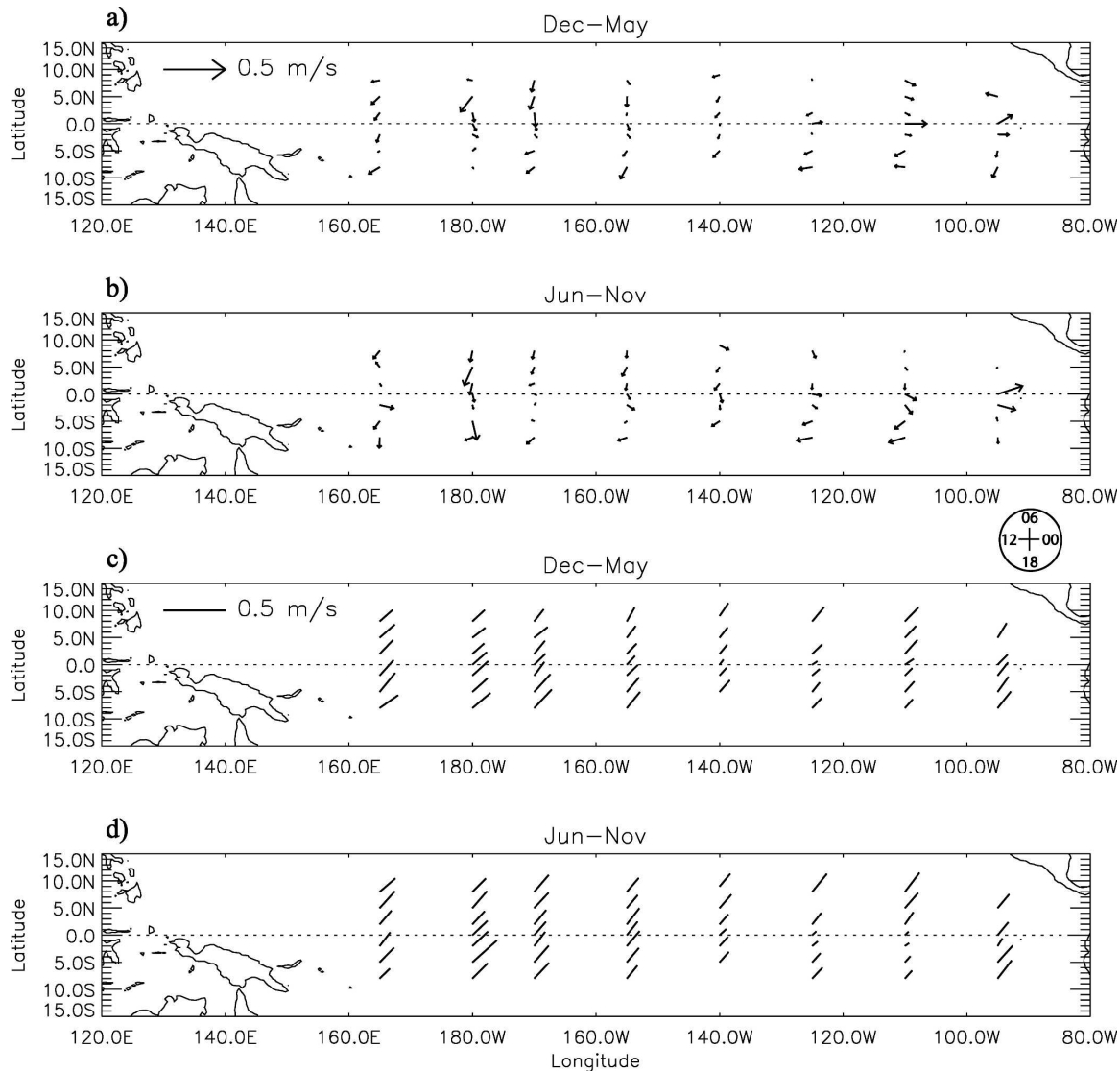


FIG. 5. December–May and June–November amplitudes and phases of the (a), (b) diurnal and (c), (d) semidiurnal harmonics of the zonal wind. The length of each vector represents amplitude of the corresponding harmonic [scales at top-left corners of (a) and (c)] and the direction represents the LT of maximum westerly wind anomaly (clock at middle right).

November than in the annual mean and December–May (Figs. 2b and 5c,d). The diurnal meridional wind harmonics are also seasonally dependent, with larger amplitudes in June–November than in December–May (Figs. 6a,b). The enhancement is particularly evident over the eastern basin.

Averaged over the buoy array, the daily zonal and meridional wind cycles are dominated by semidiurnal and diurnal variability, respectively, for both semianual means (Fig. 7). The basin-averaged amplitude of the semidiurnal zonal wind harmonics does not vary significantly from season to season, while that of the diurnal meridional wind harmonics is clearly larger dur-

ing June–November compared with December–May. The semidiurnal variability of the zonal wind component and the diurnal variability of the meridional wind component are analyzed further, as they dominate the climatological daily mean wind cycle over the tropical Pacific Ocean.

#### 4. Discussion

##### a. Semidiurnal variability

In the absence of friction and nonlinear effects, the momentum balance for the zonal wind component may be expressed as

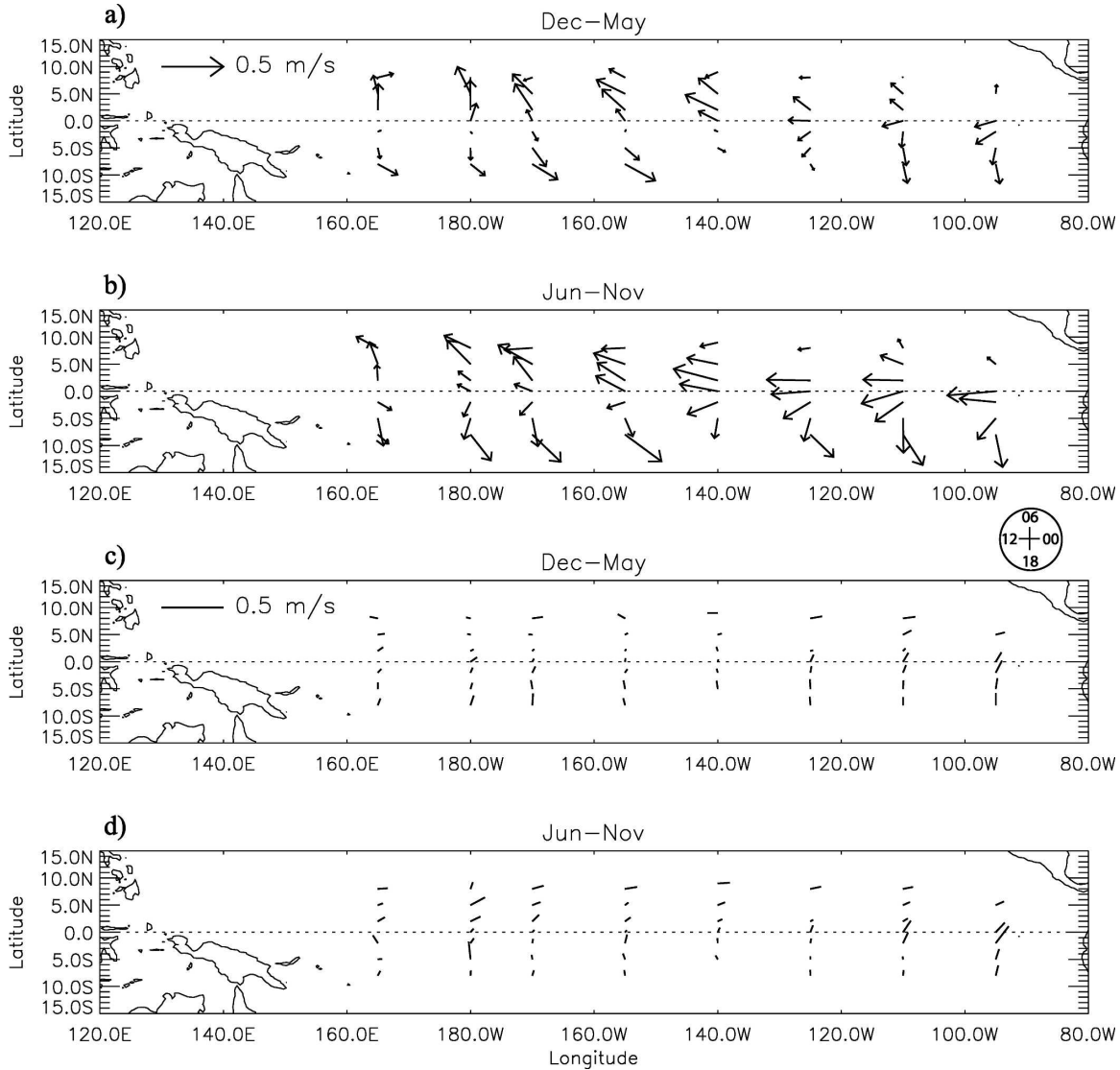


FIG. 6. Same as in Fig. 5, but for the meridional wind. The direction of the vectors represents the LT of maximum southerly wind anomaly (clock at middle right).

$$\frac{\delta u}{\delta t} = -\frac{1}{\rho} \frac{\delta p}{\delta x} + fv, \quad (2)$$

where the zonal wind acceleration ( $\delta u/\delta t$ ) is associated with the pressure gradient in the east–west direction ( $\delta p/\delta x$ ), the density of air ( $\rho = 1.2 \text{ kg m}^{-3}$ ), and the Coriolis force ( $fv$ , where  $f$  is the Coriolis parameter and  $v$  is the meridional wind). We use Eq. (2) to assess whether the observed semidiurnal zonal wind variations over the tropical Pacific are consistent with those derived from the local pressure gradient force associated with atmospheric thermal tides.

Classical atmospheric thermal tidal theory (e.g., Chapman and Lindzen 1970) predicts a zonally uniform

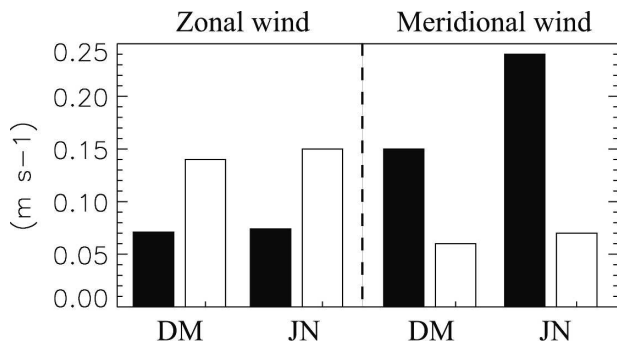


FIG. 7. Same as in Fig. 4, but for semiannual mean amplitudes: December–May (DM) and June–November (JN).

semidiurnal pressure wave in the tropics. Haurwitz and Cowley (1973, hereafter HC) show that the amplitude and phase of the semidiurnal pressure variability are relatively constant within  $20^\circ$  of the equator, with values  $\sim 1$  hPa and  $\sim 0945/2145$  LT, respectively. Their formula for the annual mean semidiurnal surface pressure variation based on zonally averaged land station records is

$$p = 1.161 \cos^3(\theta) \sin(2t + 159^\circ), \quad (3)$$

where  $\theta$  is latitude and  $t$  is local time in degrees (i.e., one day is divided into 360 equal parts). Since HC approximated the global distribution of the semidiurnal pressure wave based only on land station data, the accuracy of their results over the ocean is questionable. Nevertheless, ship measurements of sea level pressure over the tropical Pacific ( $9^\circ\text{N}$ – $9^\circ\text{S}$ ,  $162.5^\circ\text{E}$ – $92.5^\circ\text{W}$ ) from the COADS as analyzed by Dai and Wang (1999, hereafter DW) indicate semidiurnal pressure variations of similar spatially uniform amplitude and phase ( $\sim 1$  hPa and  $\sim 0950/2150$  LT, respectively).

We use the pressure data analyzed by DW, available as seasonal (3 month) and annual mean amplitudes and phases of the diurnal and semidiurnal harmonics on a  $2^\circ$  latitude  $\times$   $5^\circ$  longitude grid, and we use the semidiurnal surface pressure formula from HC [Eq. (3)] to compute the semidiurnal variation of the zonal wind component from our Eq. (2). The pressure harmonics analyzed by DW were first smoothed along the latitude and longitude directions using a 4-point boxcar average. The smoothed pressure harmonics were then used to reconstruct the daily pressure marches at each grid point and the zonal pressure gradients centered at the TAO buoy locations were computed (e.g., the zonal pressure gradient for the buoys at  $165^\circ\text{E}$  was approximated by the pressure difference between DW pressure data at  $167.5^\circ$  and  $162.5^\circ\text{E}$ ). Two neighboring pressure gradients in the longitude direction were averaged for buoys situated at the midpoints of the DW pressure grid (e.g., pressure gradients computed at  $1^\circ\text{N}$  and  $1^\circ\text{S}$  were averaged to obtain the pressure gradient for the buoys along the equator). All available meridional wind data, including those of buoys with  $<50\%$  data coverage (Table 1), were used to compute the Coriolis term in Eq. (2).

The annual mean semidiurnal variability of the observed zonal wind averaged over all buoys in the tropical Pacific agrees well with those derived from the two pressure data sources, although the observed amplitude is smaller than the pressure-derived amplitudes ( $0.14$  versus  $0.20$   $\text{m s}^{-1}$ ; Fig. 8a). Differences in the amplitudes between the observed and pressure-derived zonal

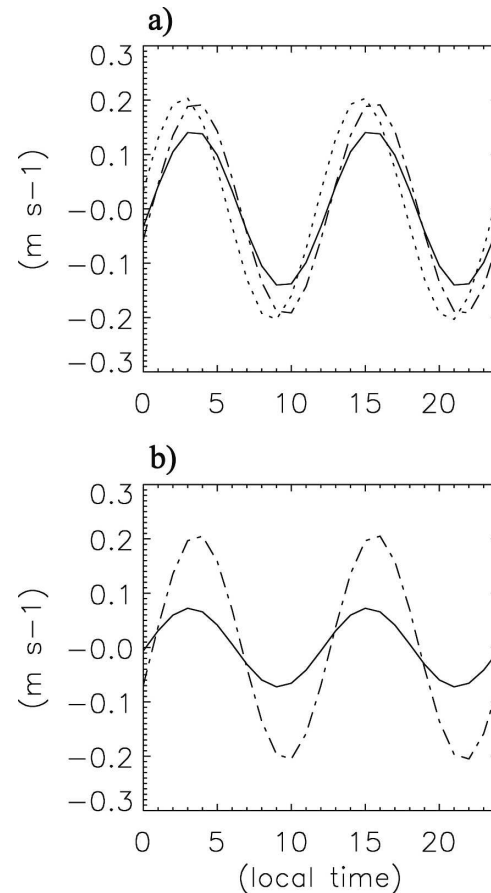


FIG. 8. (a) Comparison of semidiurnal zonal wind averaged over the tropical Pacific ( $\sim 9^\circ\text{N}$ – $9^\circ\text{S}$ ,  $165^\circ\text{E}$ – $95^\circ\text{W}$ ): observed from TAO array (solid) and derived from sea level pressure measurements from DW COADS data (dash-dot) and from HC land station records (dot). (b) Same as (a), but averaged over the eastern equatorial Pacific ( $\sim 1^\circ\text{N}$ – $5^\circ\text{S}$ ,  $125^\circ$ – $110^\circ\text{W}$ ).

winds may be due to neglected effects of surface friction and nonlinear terms in the momentum balance as well as measurement errors. Comparisons of the seasonal averages of the observed and pressure-derived winds are similar to the annual mean results (not shown). We note that the lack of seasonal variation in the semidiurnal zonal wind and pressure harmonics is consistent with atmospheric thermal tidal theory (Chapman and Lindzen 1970; HC).

Next we examine whether the reduction in amplitude of the semidiurnal zonal wind harmonics along  $125^\circ$  and  $110^\circ\text{W}$  at, and south of, the equator is reflected in the pressure field. The semidiurnal zonal wind amplitude derived from the pressure data of DW in the region ( $1^\circ\text{N}$ – $5^\circ\text{S}$ ,  $127.5^\circ$ – $107.5^\circ\text{W}$ ) is the same as the basinwide average ( $0.20$   $\text{m s}^{-1}$ ) and is thus considerably larger than observed ( $0.07$   $\text{m s}^{-1}$ ; Fig. 8b). Note that regional pressure information is not available from HC. The

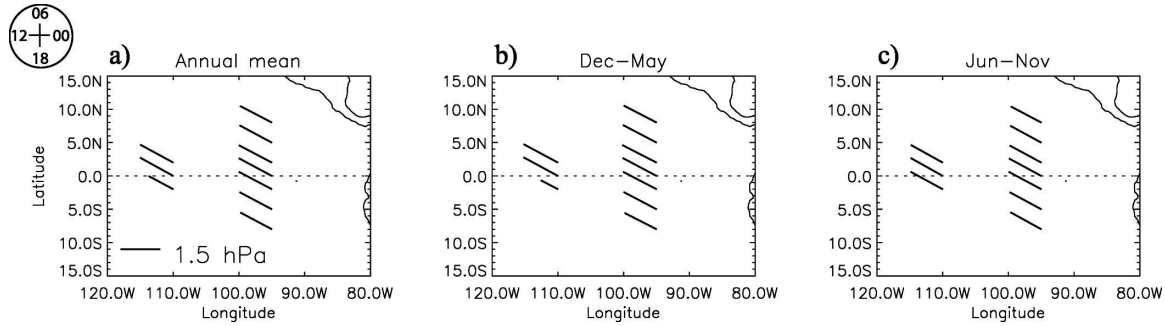


FIG. 9. Amplitudes and phases of semidiurnal harmonics of sea level pressure: (a) annual mean, (b) December–May, and (c) June–November. The length of each vector represents amplitude of the corresponding harmonic [scale at bottom-left corner of (a)] and the direction represents the LT of pressure anomaly maximum (clock at top left).

spatial coverage of the TAO buoy pressure data ( $2^{\circ}\text{N}$ – $2^{\circ}\text{S}$  along  $110^{\circ}\text{W}$  and  $8^{\circ}\text{N}$ – $8^{\circ}\text{S}$  along  $95^{\circ}\text{W}$ ) is too limited to allow a meaningful assessment of the semidiurnal zonal pressure gradient force. However, the observed semidiurnal pressure harmonic field (Fig. 9) shows no evidence of a reduction in amplitude at the locations where the semidiurnal zonal wind harmonic is suppressed, except for the buoy at  $2^{\circ}\text{S}$ ,  $110^{\circ}\text{W}$  in December–May (however, this estimate is based on only 16% data coverage during 2000–04; Table 1). Indeed, the semidiurnal pressure harmonics from the TAO buoys are highly uniform in both amplitude and phase ( $\sim 1.4$  hPa and  $\sim 1010/2210$  LT, respectively) for annual and semiannual means (Fig. 9).

Since it appears that the zonal pressure gradient force cannot account for the reduction in semidiurnal zonal wind amplitude over the cold surface waters in the eastern Pacific, as an alternative mechanism we explore a possible role of enhanced boundary layer stability that may attenuate the surface wind amplitude by inhibiting the vertical mixing of momentum. Boundary layer stability has been shown to affect the strength of near-surface winds in the eastern equatorial Pacific on a variety of time scales from annual to subseasonal (Wallace et al. 1989; Chelton et al. 2001; Xie 2004). Clearly, a full investigation of the role of boundary layer stability and associated boundary layer depth requires observations of the vertical structure of the semidiurnal zonal wind cycle, information not currently available over the tropical Pacific Ocean. However, as a first step, we analyzed the spatial structure of atmospheric boundary layer stability as estimated from the difference between long-term daily mean SST and air temperature from the TAO buoys.

SSTs exceed near-surface air temperatures over the entire domain in the annual and semiannual means, reflecting that the tropical marine boundary layer is generally unstable (Fig. 10). However, the magnitude

of the SST–air temperature difference is greatly diminished over the cold surface waters of the eastern equatorial upwelling zone and southeast tropical Pacific, approaching near-zero values in the cold season (June–November; Fig. 10c). This reduction of boundary layer instability (or relative enhancement of boundary layer stability) is consistent with the prevalence of stratiform low clouds at, and south of, the equator in the eastern Pacific (Deser et al. 1993; Norris 1998). The annual and semiannual distributions of mean boundary layer stability (Fig. 10) compare well with those of semidiurnal zonal wind amplitude (Figs. 2b and 5c,d): their pattern correlation coefficients are in the range of 0.7–0.8. In particular, the region of enhanced stability over the eastern Pacific is associated with a reduction in semidiurnal amplitude. This correspondence is confirmed by a scatterplot between seasonal (3 month) mean boundary layer stability and semidiurnal zonal wind amplitude, which reveals a strong positive relationship for SST–air temperature differences  $< 0.6^{\circ}\text{C}$  (e.g., buoys in the eastern Pacific; Fig. 11). Whether the similarity between the spatial patterns of mean boundary layer stability and semidiurnal zonal wind harmonic amplitude is causal or incidental remains to be seen.

One source of information on the vertical structure of the daily wind cycle is the lower-tropospheric wind profiler at Isla San Cristóbal in the Galápagos Islands ( $0.90^{\circ}\text{S}$ ,  $89.61^{\circ}\text{W}$ ), which provides half-hourly wind data between 300 and 2600 m. Using these data, HD found that the daily cycle of winds below  $\sim 500$  m is decoupled from that aloft during periods of low ( $< 23^{\circ}\text{C}$ ) SST. However, contrary to our findings, higher-amplitude semidiurnal zonal wind signals were observed near the surface during periods of increased boundary layer stability, and these were speculated to be due to water vapor tidal forcing in the lowest 500 m (HD). Further work is needed to reconcile the different dependencies of the semidiurnal zonal wind amplitudes

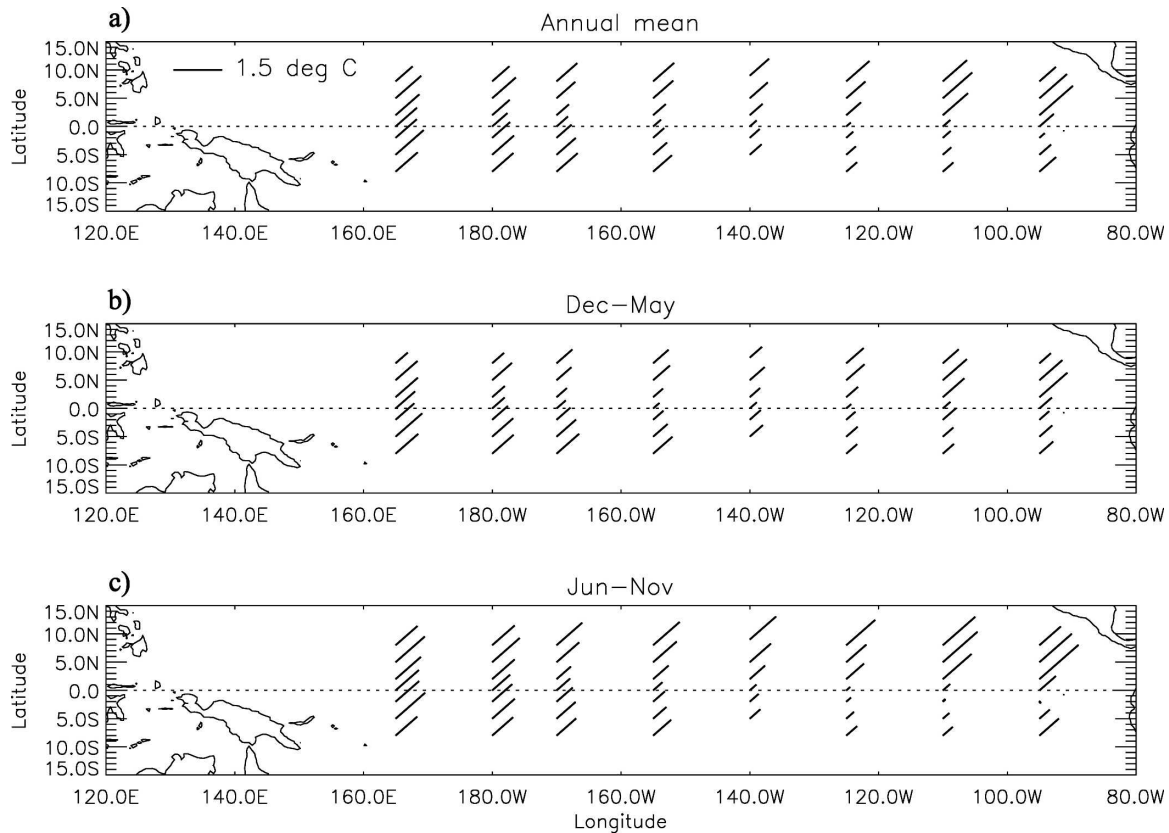


FIG. 10. Long-term daily mean boundary layer stability (daily mean SST minus air temperature) during 1993–2004: (a) annual mean, (b) December–May, and (c) June–November. Scale at top-left corner of (a). Small vectors (i.e., small temperature differences) indicate enhanced stability. Directions of the bars are arbitrary.

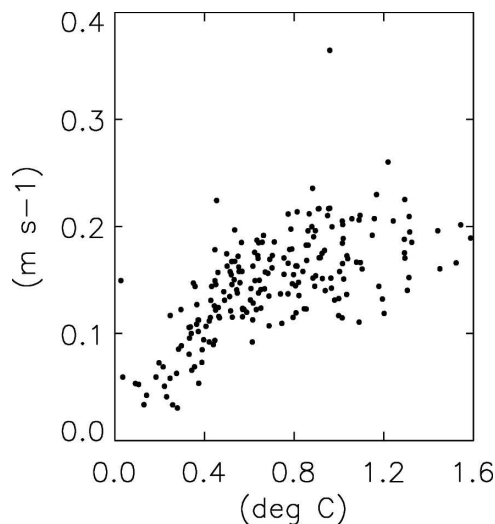


FIG. 11. Scatterplot of the seasonal (3 month) mean boundary layer stability (daily mean SST minus air temperature in  $^{\circ}\text{C}$ ) vs the seasonal mean semidiurnal amplitude ( $\text{m s}^{-1}$ ) of zonal wind at all 51 buoys. Dots in the bottom-left quadrant represent data from eastern equatorial buoys.

on boundary layer stability in the Galápagos profiler and TAO buoy data.

#### b. Diurnal variability

The spatial pattern of the diurnal meridional wind harmonics is more complex than that of the semidiurnal zonal wind harmonics. Diurnal meridional wind variations tend to be out of phase north and south of the equator (southerly wind anomaly maxima  $\sim 0700$  LT at  $5^{\circ}\text{N}$  and  $\sim 1900$  LT at  $5^{\circ}\text{S}$ ), while on the equator in the eastern Pacific, southerly wind anomaly maxima occur around noon, particularly during the cold season (June–November; Fig. 6b). We note that the noon phase and seasonal dependence of the amplitude of the diurnal meridional wind variations in the eastern equatorial Pacific are consistent with the Galápagos wind profiler results of HD.

Following the same method used to analyze the semidiurnal zonal wind variability, we compare the observed diurnal meridional wind variability with that derived from the diurnal pressure harmonics of DW

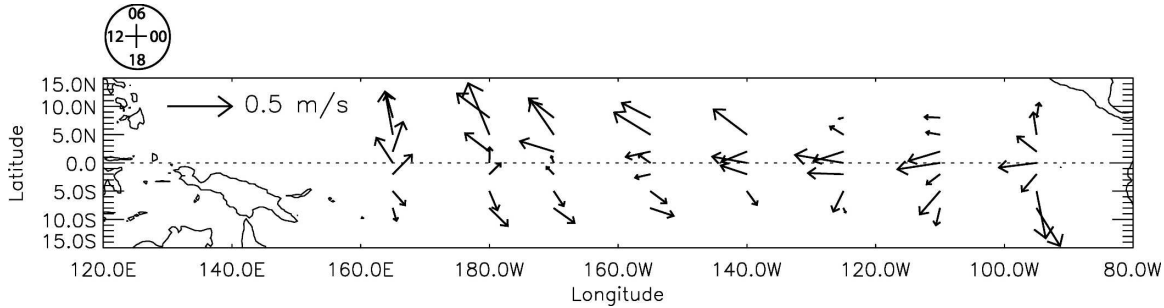


FIG. 12. Annual mean amplitudes and phases of the diurnal harmonics of the meridional wind derived from DW COADS pressure data based on Eq. (4). The length of each vector represents amplitude (scale at top-left corner) and the direction represents the LT of maximum southerly wind anomaly (clock at top left).

(smoothed as described in section 4a) based on the momentum balance for the meridional wind component:

$$\frac{\delta v}{\delta t} = -\frac{1}{\rho} \frac{\delta p}{\delta y} - fu. \quad (4)$$

The annual mean spatial patterns of the observed and pressure-derived diurnal meridional wind harmonics are qualitatively similar, with opposite phases in the Northern and Southern Hemispheres of the western Pacific ( $\sim 0600\text{--}0900$  and  $1800\text{--}2100$  LT, respectively) and approximately noon phases at the equator in the eastern Pacific (Figs. 3a and 12). The annual mean amplitudes tend to be 15% larger for the pressure-derived harmonics than the observed harmonics. Semiannual mean patterns of the pressure-derived diurnal meridional wind harmonics are also largely consistent with those of the TAO winds (not shown). The good agreement between the observed and pressure-derived wind harmonics indicate that the pressure gradient force plays an important, if not dominant, role in determining the diurnal cycle of the meridional winds over the tropical Pacific, while other factors such as boundary layer stability may be of secondary importance.

Hourly wind vector snapshots representing departures from the daily mean winds, reconstructed from the amplitudes and phases of the diurnal zonal and meridional wind harmonics, are shown at 3-h intervals from 0100 to 1300 LT for the June–November season in Fig. 13 (results based on annual and December–May means exhibit similar patterns with generally smaller amplitudes; not shown). These snapshots confirm the remarkable asymmetry of the diurnal meridional wind component about the equator, especially in the western Pacific. This pattern results in enhanced equatorial divergence  $\sim 0700$  LT (convergence  $\sim 1900$  LT). There is also an indication of a diurnal cycle in surface wind divergence along the southern border of the ITCZ that

is out of phase with the one on the equator, although the spatial coverage of the TAO array is not sufficient to fully delineate this feature.

The diurnal cycles of wind divergence relative to the daily mean along the near-ITCZ ( $8^{\circ}\text{--}5^{\circ}\text{N}$ ) and near-equatorial ( $0^{\circ}\text{--}2^{\circ}\text{S}$ ; similar results are obtained for  $2^{\circ}\text{N}\text{--}2^{\circ}\text{S}$ ) bands for December–May and June–November are shown in Fig. 14. Solid lines denote zonal averages across the tropical Pacific ( $165^{\circ}\text{E}\text{--}95^{\circ}\text{W}$ ) and dashed lines denote averages for the western basin ( $165^{\circ}\text{E}\text{--}155^{\circ}\text{W}$ ). All available wind data within the domains, including those of buoys with  $<50\%$  data coverage (Table 1), were used to compute the divergence. The diurnal cycles in the near-ITCZ and near-equatorial bands are approximately out of phase in both seasons and longitudinal domains, with maximum equatorial divergence (ITCZ convergence) at  $0700\text{--}0900$  LT, consistent with Fig. 13. In addition, they are slightly larger in amplitude and earlier in phase over the western basin than the full tropical Pacific, also consistent with the wind vectors in Fig. 13. In the western Pacific, the diurnal amplitude of the near-equatorial divergence is  $7.1 \times 10^{-7} \text{ s}^{-1}$  in December–May, similar to the value for June–November ( $8.0 \times 10^{-7} \text{ s}^{-1}$ ), while that of the near-ITCZ divergence is  $6.2 \times 10^{-7} \text{ s}^{-1}$  in December–May, larger than the value for June–November ( $3.6 \times 10^{-7} \text{ s}^{-1}$ ). We speculate that the smaller diurnal amplitude of the near-ITCZ divergence in June–November may be due to the more northerly position of the mean ITCZ in that season such that the TAO buoy domain does not fully capture the associated low-level convergence (recall Fig. 1).

The out-of-phase relationship between the diurnal cycles of surface wind divergence for the near-ITCZ and near-equatorial regions suggests that the two may be linked through a diurnally oscillating meridional overturning circulation, at least in the western Pacific where the diurnal wind harmonics exhibit a relatively

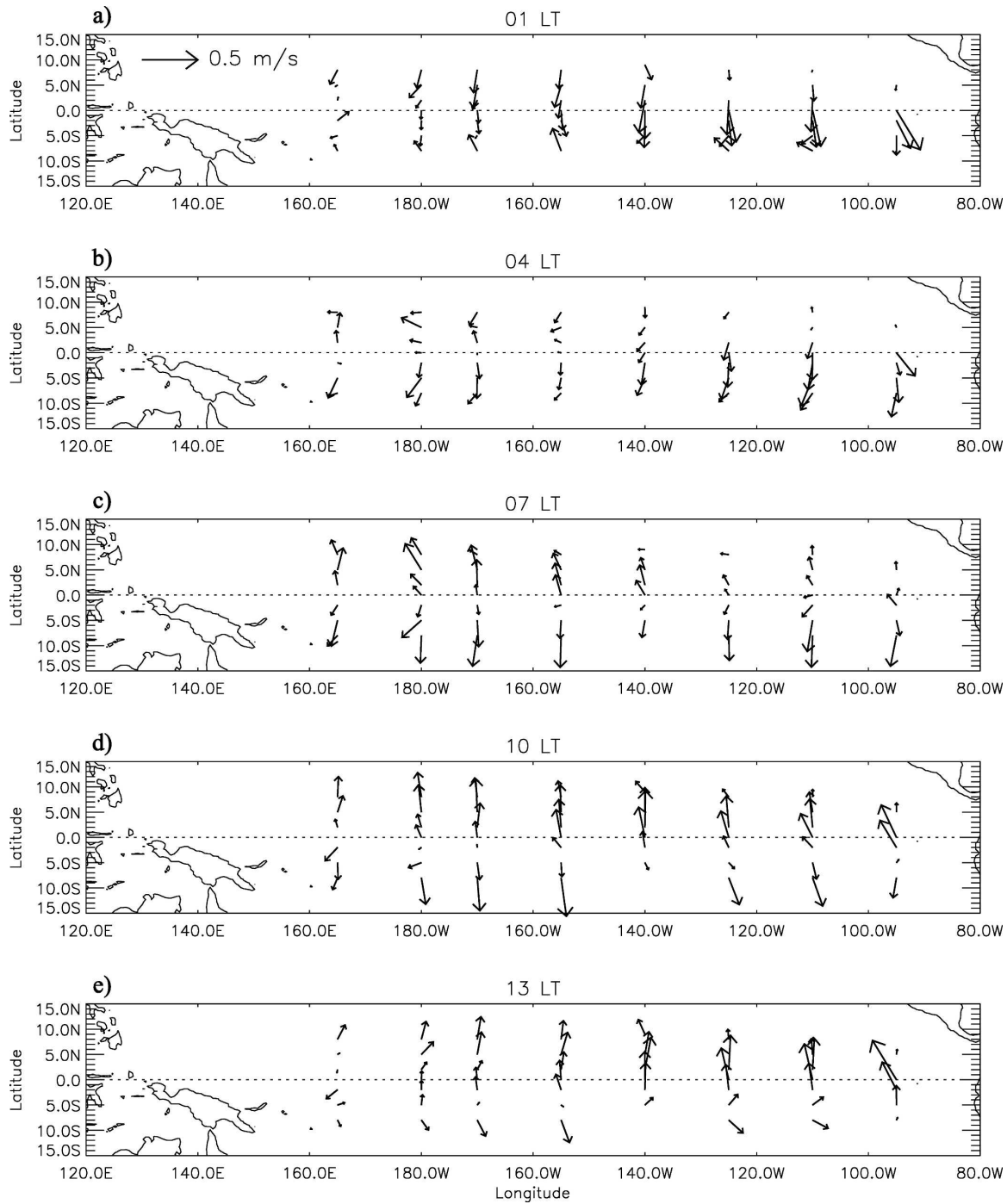


FIG. 13. June–November wind vector departures from the daily means reconstructed from the diurnal harmonics at (a) 0100, (b) 0400, (c) 0700, (d) 1000, and (e) 1300 LT. Scale is shown at top-left corner of (a).

simple pattern (see also DS). Although it remains to be seen how this diurnal surface wind divergence pattern relates to diurnal precipitation changes over the tropical Pacific, the early morning maximum in rainfall reported in numerous studies (Gray and Jacobson 1977; Hendon and Woodberry 1993; Janowiak et al. 1994;

Serra and McPhaden 2004; Bowman et al. 2005; Yang and Smith 2006) appears to be broadly consistent with the morning maximum in surface wind convergence into the western Pacific ITCZ. Furthermore, a simple estimate of the magnitude of the diurnal rainfall change expected from the amplitude of the diurnal surface

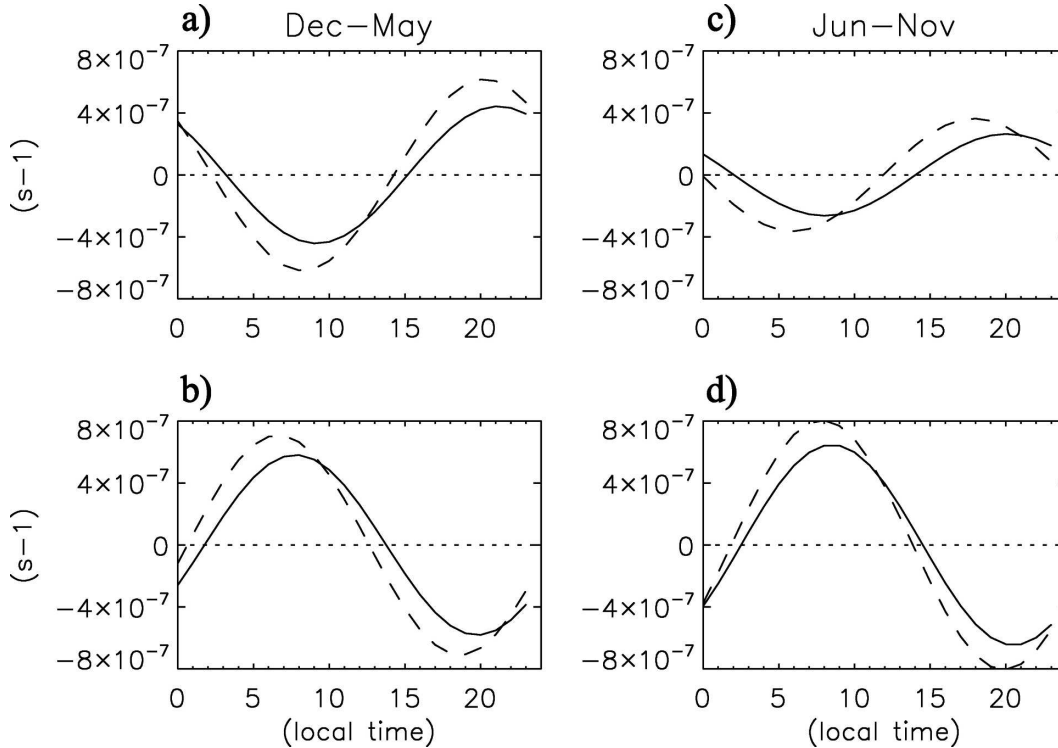


FIG. 14. (left) December–May and (right) June–November diurnal cycle (LT) of surface wind divergence ( $s^{-1}$ ) averaged over all longitudes ( $165^{\circ}\text{E}$ – $95^{\circ}\text{W}$ ; solid) and western longitudes ( $165^{\circ}\text{E}$ – $155^{\circ}\text{W}$ ; dashed) for (a), (c) near-ITCZ ( $8^{\circ}$ – $5^{\circ}\text{N}$ ) and (b), (d) near-equatorial ( $0^{\circ}$ – $2^{\circ}\text{S}$ ) regions. All available wind data (including buoys with  $<50\%$  data coverage, Table 1) were analyzed. The daily means at each buoy have been removed. Positive (negative) values indicate divergence (convergence) relative to the daily mean.

wind divergence compares favorably with the observed amplitude of diurnal rainfall variations (DS). However, a joint analysis of diurnal precipitation and wind variability is needed to link the two processes more definitively.

As we have shown, the pattern of diurnal meridional wind variations from the TAO buoys is generally consistent with the diurnal pressure gradient force. The zonally symmetric portion of the pressure gradient force that results in out-of-phase meridional wind variations north and south of the equator appears to be consistent with the structure of the diurnal atmospheric thermal tide (Braswell and Lindzen 1998; DW). The diurnal component of sea level pressure variability over the eastern Pacific cold tongue that drives the noon equatorial southerly wind maximum may result from the diurnal cycle of SST and associated atmospheric boundary layer specific humidity. We note that this mechanism would account for the confinement of the noon southerly wind maximum below  $\sim 500$  m during periods of low SST at the Galápagos Islands as documented by HD. Further work is needed to explore these mechanisms more fully.

## 5. Conclusions

The diurnal and semidiurnal variations of the zonal and meridional near-surface wind components over the tropical Pacific presented in this study generally agree with the findings of DS, which were based on a smaller sample of years (1993–96 versus 1993–2004). In particular, we confirm that the zonal wind variability is mainly semidiurnal, with near-uniform amplitude ( $\sim 0.14$   $\text{m s}^{-1}$ ) and phase (maximum westerly wind anomalies  $\sim 0325/1525$  LT) across the basin (except the eastern equatorial Pacific) in all seasons. This semidiurnal zonal wind pattern is well explained by classical atmospheric thermal tidal theory. We also confirm that the meridional wind variability is mainly diurnal, and tends to be out of phase north and south of the equator (maximum southerly wind anomalies  $\sim 0700$  LT at  $5^{\circ}\text{N}$  and  $\sim 1900$  LT at  $5^{\circ}\text{S}$ ) particularly over the western Pacific, while on the equator in the eastern Pacific, there is a noon southerly wind anomaly maximum. In the eastern Pacific ( $125^{\circ}$ – $95^{\circ}\text{W}$ ), the diurnal meridional wind cycle exhibits a southward phase progression from  $5^{\circ}\text{N}$  to  $8^{\circ}\text{S}$ .

We have shown that the amplitudes of the diurnal meridional wind variations are larger during the cold season (June–November) than the warm season (December–May), with similar spatial patterns in the two seasons. The diurnal meridional wind variations over the western Pacific result in enhanced (relative to the daily mean) divergence along the equator and convergence along the southern border of the ITCZ at  $\sim 0700$  LT, with opposite conditions at  $\sim 1900$  LT. The amplitude of the diurnal cycle in surface wind divergence is  $4\text{--}8 \times 10^{-7} \text{ s}^{-1}$  depending on region and season, similar to that found by DS.

The spatial pattern of the diurnal meridional wind variations agrees well with that derived from the diurnal pressure harmonics of DW, suggesting the dominant role of the pressure gradient force in determining the diurnal cycle of the meridional winds over the tropical Pacific. Further work is needed to understand the processes contributing to the diurnal pressure gradient force, including the role of atmospheric thermal tides, diurnal SST variations, and diurnal variations in deep convection. In this regard, improved observations of the vertical structure of diurnal wind variations, as well as an overarching investigation that examines the diurnal wind variability in conjunction with that of deep convection and precipitation over the tropical oceans, would be beneficial.

One result that is more prominent in our study compared with DS is the suppression the semidiurnal zonal wind amplitude at and south of the equator in the eastern Pacific. This feature is most striking during the cold season (June–November), which is why it was only hinted at in the annual mean analyses of DS. Based on the available sea level pressure data, we found no evidence for a concomitant reduction of the semidiurnal zonal pressure gradient force, leading us to propose an alternative mechanism, namely a reduction of vertical momentum mixing due to enhanced boundary layer stability over the cold surface waters. Although we have no direct evidence for this mechanism, we note that the spatial patterns of boundary layer stability (estimated from the long-term daily mean SST–air temperature difference) and semidiurnal zonal wind amplitude are similar, as are their seasonal dependencies. Additional evidence is required to support or refute this hypothesis. In particular, observations of the vertical structure of semidiurnal wind variations are needed to improve our understanding of the role of boundary layer processes in downward-propagating tidal signals.

*Acknowledgments.* This work began under the auspices of the Significant Opportunities in Atmospheric Research and Science (SOARS) program of the Uni-

versity Corporation for Atmospheric Research, with funding from the National Science Foundation, the U.S. Department of Energy, the National Oceanic and Atmospheric Administration, and the NASA Goddard Space Flight Center. It was completed in the Department of Atmospheric Sciences at University of Washington under the guidance of Dr. John M. Wallace, who is acknowledged for his invaluable comments. We thank Dr. Aiguo Dai for providing and sharing his expertise in the COADS pressure data, Mr. Adam Phillips for his generous assistance with data processing, and two anonymous reviewers for many constructive suggestions. We also thank NOAA/Pacific Marine Environmental Laboratory for providing the TAO data and the TAO–EPIC Project for providing the TAO pressure data. Financial support was provided in part by the SOARS program and the National Science Foundation Graduate Research Fellowship.

#### REFERENCES

- Bowman, K. P., J. C. Collier, G. R. North, Q. Wu, E. Ha, and J. Hardin, 2005: Diurnal cycle of tropical precipitation in Tropical Rainfall Measuring Mission (TRMM) satellite and ocean buoy rain gauge data. *J. Geophys. Res.*, **110**, D21104, doi:10.1029/2005JD005763.
- Braswell, W. D., and R. S. Lindzen, 1998: Anomalous short wave absorption and atmospheric tides. *Geophys. Res. Lett.*, **25**, 1293–1296.
- Chapman, S., and R. S. Lindzen, 1970: *Atmospheric Tides*. D. Reidel, 200 pp.
- Chelton, D. B., and Coauthors, 2001: Observations of coupling between surface wind stress and sea surface temperature in the eastern tropical Pacific. *J. Climate*, **14**, 1479–1497.
- Dai, A., and J. Wang, 1999: Diurnal and semidiurnal tides in global surface pressure fields. *J. Atmos. Sci.*, **56**, 3874–3891.
- Deser, C., and C. A. Smith, 1998: Diurnal and semidiurnal variations of the surface wind field over the tropical Pacific Ocean. *J. Climate*, **11**, 1730–1748.
- , J. J. Bates, and S. Wahl, 1993: The influence of sea surface temperature gradients on stratiform cloudiness along the equatorial front in the Pacific Ocean. *J. Climate*, **6**, 1172–1180.
- Draper, N. R., and H. Smith, 1966: *Applied Regression Analysis*. John Wiley and Sons, 407 pp.
- Gray, W. M., and R. W. Jacobson Jr., 1977: Diurnal variation of deep cumulus convection. *Mon. Wea. Rev.*, **105**, 1171–1188.
- Gutzler, D. S., and L. M. Hartten, 1995: Daily variability of lower tropospheric winds over the tropical western Pacific. *J. Geophys. Res.*, **100** (D11), 22 999–23 008.
- Hamilton, K., 1980: The geographical distribution of the solar semidiurnal surface pressure oscillation. *J. Geophys. Res.*, **85**, 1945–1949.
- Hartten, L. M., and P. A. Datulayta, 2004: Seasonal and interannual variations in the daily cycle of winds over the Galápagos. *J. Climate*, **17**, 4522–4530.
- Haurwitz, B., 1964: Atmospheric tides. *Science*, **144**, 1415–1422.
- , and A. D. Cowley, 1973: The diurnal and semidiurnal baro-

- metric oscillations, global distribution and annual variation. *Pure Appl. Geophys.*, **102**, 193–222.
- Hendon, H. H., and K. Woodberry, 1993: The diurnal cycle of tropical convection. *J. Geophys. Res.*, **98** (D9), 16 623–16 637.
- Janowiak, J. E., P. A. Arkin, and M. Morrissey, 1994: An examination of the diurnal cycle in oceanic tropical rainfall using satellite and in situ data. *Mon. Wea. Rev.*, **122**, 2296–2311.
- Lindzen, R. S., 1967: Thermally driven diurnal tide in the atmosphere. *Quart. J. Roy. Meteor. Soc.*, **93**, 18–42.
- Norris, J. R., 1998: Low cloud type over the ocean from surface observations. Part II: Geographical and seasonal variations. *J. Climate*, **11**, 383–403.
- Serra, Y. L., and M. J. McPhaden, 2004: In situ observations of diurnal variability in rainfall over the tropical Pacific and Atlantic Oceans. *J. Climate*, **17**, 3496–3509.
- Wallace, J. M., T. P. Mitchell, and C. Deser, 1989: The influence of sea surface temperature on surface wind in the eastern equatorial Pacific: Seasonal and interannual variability. *J. Climate*, **2**, 1492–1498.
- Xie, S.-P., 2004: Satellite observations of cool ocean–atmosphere interaction. *Bull. Amer. Meteor. Soc.*, **85**, 195–208.
- Yang, G.-Y., and J. Slingo, 2001: The diurnal cycle in the Tropics. *Mon. Wea. Rev.*, **129**, 784–801.
- Yang, S., and E. A. Smith, 2006: Mechanisms for diurnal variability of global tropical rainfall observed from TRMM. *J. Climate*, **19**, 5190–5226.